Optical Control of Slow Topological Electrons in Moiré Systems

Christopher Yang,[1] Iliya Esin,[1] Cyprian Lewandowski,[1,2,3] and Gil Refael[1]
[1]Department of Physics, IQIM, California Institute of Technology, Pasadena, California 91125, USA
[2]National High Magnetic Field Laboratory, Tallahassee, Florida 32310, USA
[3]Department of Physics, Florida State University, Tallahassee, Florida 32306, USA

(Received 1 February 2023; revised 17 May 2023; accepted 13 June 2023; published 13 July 2023)

Floquet moiré materials possess optically-induced flat-electron bands with steady-states sensitive to drive parameters. Within this regime, we show that strong interaction screening and phonon bath coupling can overcome enhanced drive-induced heating. In twisted bilayer graphene (TBG) irradiated by a terahertz-frequency continuous circularly polarized laser, the extremely slow electronic states enable the drive to control the steady state occupation of high-Berry curvature electronic states. In particular, above a critical field amplitude, high-Berry-curvature states exhibit a slow regime where they decouple from acoustic phonons, allowing the drive to control the anomalous Hall response. Our work shows that the laser-induced control of topological and transport physics in Floquet TBG are measurable using experimentally available probes.

DOI: 10.1103/PhysRevLett.131.026901

Introduction.—Time-periodic fields can drive materials into exotic nonequilibrium phases [1–15], with unconventional transport and optical characteristics [16–23] controllable by external parameters. In laser-driven twisted bilayer graphene (TBG) [24–28], a flat-band regime with pronounced electron-electron interaction effects is accessible away from the magic angles [29]. Generating low-temperature Floquet states in such a regime requires cooling processes that compensate for strong drive-induced electron-electron heating. A common cooling solution involves coupling Floquet systems to low-temperature phonon baths [3,30,31].

We demonstrate that intrinsic electron-phonon coupling in TBG and Coulomb screening can stabilize low-temperature steady states in Floquet TBG under terahertz (THz) frequency, circularly polarized laser drives. In this steady state, the drive amplitude controls the filling of electronic states with large Berry curvature, resulting in a highly tunable anomalous conductivity σ_{xy} [16,32–35] [Figs. 1(a) and 1(b)]. The ability to tune the Floquet steady-state results from the unique slow electron regime in TBG where phonons travel faster than—and decouple from—many flat band electronic states [36,37].

The system.—We begin by constructing the time-periodic, interacting Hamiltonian for laser-driven TBG near the charge neutrality point and at a twist angle θ. The single-particle effective Hamiltonian of undriven TBG is $\hat{H}_0 = \sum_{\boldsymbol{k}\nu\xi} E^{(\xi)}_{\boldsymbol{k}\nu} \hat{c}^{(\xi)\dagger}_{\boldsymbol{k}\nu} \hat{c}^{(\xi)}_{\boldsymbol{k}\nu}$, where $\hat{c}^{(\xi)\dagger}_{\boldsymbol{k}\nu}$ creates a Bloch state $|\xi\nu\boldsymbol{k}\rangle$ of crystal momentum $\boldsymbol{k}$, band ν, and energy $E^{(\xi)}_{\boldsymbol{k}\nu}$, near valley index $\xi = \pm 1$ of the single-layer graphene Brillouin zone [29,38]. The index $\nu = \pm$ labels the narrow central particle and hole bands [Figs. 2(a) and 2(b)] with total bandwidth W, which are separated by a large energy gap from all other bands. We consider a circularly polarized laser of vector potential $\boldsymbol{A}(t) = (\mathcal{E}/\Omega)[\cos(\Omega t)\hat{\boldsymbol{x}} - \sin(\Omega t)\hat{\boldsymbol{y}}]$ with electric field amplitude $\mathcal{E}$ and angular-frequency Ω, which couples to electrons by minimal coupling $\boldsymbol{k} \to \boldsymbol{k} + e\boldsymbol{A}(t)/\hbar$, resulting in the time-periodic Hamiltonian $\hat{H}_0(t)$.

The periodic Hamiltonian $\hat{H}_0(t)$ gives rise to Floquet eigenstates $|\Phi^{(\xi)}_{\boldsymbol{k}\alpha}(t)\rangle$ with quasienergies $\varepsilon^{(\xi)}_{\boldsymbol{k}\alpha}$ satisfying $|\varepsilon^{(\xi)}_{\boldsymbol{k}\alpha}| < \frac{1}{2}\hbar\Omega$. We consider the regime $W \le \hbar\Omega < 2W$ corresponding to a single photon resonance within the central TBG bands. Specifically, we consider

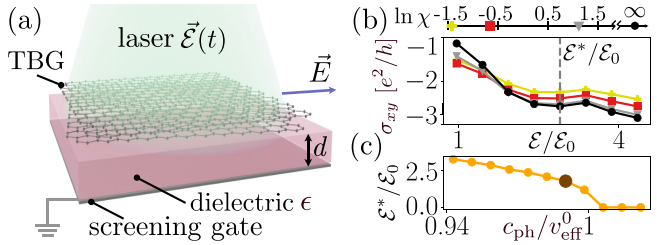

FIG. 1. (a) Schematic experimental design. Circularly polarized laser induces nontrivial Berry curvature in the narrow bands [see Figs. 2(b) and 2(c)], resulting in an anomalous Hall conductivity σ_{xy}. TBG lies on top of a dielectric and metallic gate that screen electron-electron interactions. (b) Anomalous Hall conductivity vs drive amplitude $\mathcal{E}$ for $\zeta \approx 0.5$ and various values of χ indicated on the scale [see below Eqs. (3) and (6) for definitions of ζ and χ]. The σ_{xy} features a rapid drop with $\mathcal{E}$ below the critical amplitude $\mathcal{E}^*$ (dashed line). Here, $\mathcal{E}_0 = \hbar v_F/(eL_M^2) \approx 7.2 \times 10^4$ V/m. (c) Critical amplitude vs $c_{\rm ph}/v^0_{\rm eff}$, where $v^0_{\rm eff} = v_{\rm eff}(0)$ is an effective electron velocity defined in the text. Enlarged red circle: $\mathcal{E}^*$ in (b).

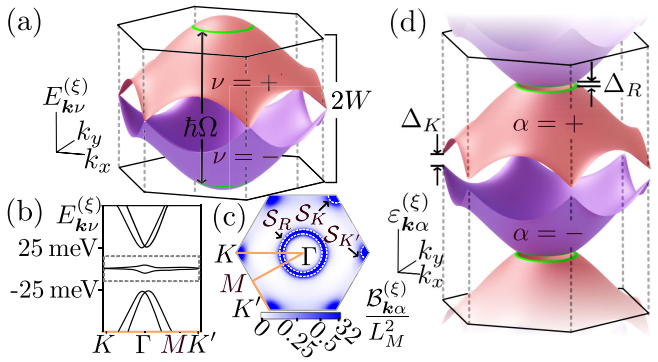

FIG. 2. (a) Enlargement of schematic narrow bands in a moiré system. Drive with angular frequency Ω resonantly couples states along resonance rings (green curves). (b) Undriven spectrum of TBG along a line in the Brillouin zone indicated by the orange curve in (c). Dashed frame encloses optically active, narrow central bands $\nu = \pm 1$. (c) Berry curvature $\mathcal{B}^{(\xi)}_{\boldsymbol{k}+}$ in the upper Floquet band, with blue color intensity proportional to $\tanh(2\mathcal{B}^{(\xi)}_{\boldsymbol{k}+}/L_M^2)$ (color bar) so $\mathcal{B}^{(\xi)}_{\boldsymbol{k}+}$ peaks are more visible. Dashed lines indicate areas enclosing $\mathcal{B}^{(\xi)}_{\boldsymbol{k}+}$ peaks at the Dirac points and resonance ring. (d) Periodic quasienergy Floquet spectrum of the driven system, having two central bands shown in (a). The Floquet spectrum exhibits the upper (UFB, $\alpha = +$) and lower (LFB, $\alpha = -$) Floquet bands, separated by off-resonant gaps Δ_K at the Dirac K, K' points and a Rabi-like gap Δ_R along the resonance ring [39–41].

$\Omega = 5$ meV$/\hbar$ and TBG at a near-magic twist angle of $\theta = 1.13°$ whose Fermi velocity $v_F \approx 17$ km/s (corresponding to $W = 5$ meV in the Bistritzer-MacDonald model [29,38]) is comparable to phonon speeds in TBG [42]. The drive mixes the two central bands $\nu = \pm 1$, resulting in quasienergies $\varepsilon^{(\xi)}_{\boldsymbol{k}\alpha}$, with upper and lower Floquet bands denoted by $\alpha = \pm$ [Fig. 2(d)] [24]. The drive opens off-resonant gaps of size $\Delta_K \approx 2e^2 v_F^2 \mathcal{E}^2/\hbar\Omega^3$ at the Dirac points K and K' of the moiré Brillouin zone and a Rabi-like gap of $\Delta_R \sim V$ along the resonance ring, which is the ring on the $\boldsymbol{k}$ plane satisfying $E^{(\xi)}_{\boldsymbol{k}+} - E^{(\xi)}_{\boldsymbol{k}-} = \hbar\Omega$ [green rings in Figs. 2(a) and 2(d)]. Here, v_F is the Fermi velocity of the undriven band structure, V is the energy scale of the drive, and the expression for Δ_K comes from the Van Vleck perturbative expansion [33,39,41,43–45].

The key component for stabilizing Floquet many-body states is the electron coupling to low-temperature longitudinal TBG acoustic phonons:

$$\hat{H}_{\text{el-ph}} = \sum_{\substack{\boldsymbol{k},\boldsymbol{q},\boldsymbol{G} \\ \nu,\nu',\xi}} M^{\nu\nu'\xi}_{\boldsymbol{k},\boldsymbol{q},\boldsymbol{G}} \hat{c}^{(\xi)\dagger}_{\boldsymbol{k}+\boldsymbol{q}+\boldsymbol{G},\nu'} \hat{c}^{(\xi)}_{\boldsymbol{k}\nu} (\hat{b}^\dagger_{\boldsymbol{q}} + \hat{b}_{-\boldsymbol{q}}) + \text{H.c.} \quad (1)$$

Here, $\boldsymbol{G}$ is a moiré Brillouin zone reciprocal lattice vector, and $M^{\nu\nu'\xi}_{\boldsymbol{k},\boldsymbol{q},\boldsymbol{G}} = D\sqrt{\hbar c_{\text{ph}} q}/(\sqrt{2A_M\rho}c_{\text{ph}})\mathcal{W}^{\xi\nu\nu'}_{\boldsymbol{k},\boldsymbol{q}+\boldsymbol{G}}$ is the matrix element with deformation potential D, moiré unit cell area $A_M = \sqrt{3}L_M^2/2$, lattice vector length $L_M = a/[2\sin(\theta/2)]$, monolayer graphene density ρ, and monolayer lattice vector length $a = 0.246$ nm. The operator $\hat{b}^\dagger_{\boldsymbol{q}}$ creates an acoustic phonon mode of momentum $\boldsymbol{q}$ with amplitude q, speed c_{ph}, and energy $\hbar c_{\text{ph}} q$. The speed of sound c_{ph} in TBG is roughly the same as that in monolayer graphene, but the small Brillouin zone in TBG folds the acoustic phonon dispersion into many branches [42]. The form-factor $\mathcal{W}^{\xi\nu\nu'}_{\boldsymbol{k},\boldsymbol{q}+\boldsymbol{G}} \equiv \langle \xi\nu'\boldsymbol{k}+\boldsymbol{q}+\boldsymbol{G}|\xi\nu\boldsymbol{k}\rangle$ captures the decreasing coupling of electrons to folded phonon branches with large $\boldsymbol{G}$ [46]. We also include electron-electron interactions:

$$\hat{H}_{\text{el-el}} = \sum_{\substack{\boldsymbol{k}_1,\boldsymbol{k}_2 \\ \boldsymbol{q},\boldsymbol{G} \\ \{\nu_i\},\xi}} V^{\{\nu_i\}\xi}_{\boldsymbol{k}_1,\boldsymbol{k}_2,\boldsymbol{q},\boldsymbol{G}} \hat{c}^{(\xi)\dagger}_{\boldsymbol{k}_1+\boldsymbol{q},\nu_1} \hat{c}^{(\xi)\dagger}_{\boldsymbol{k}_2-\boldsymbol{q},\nu_2} \hat{c}^{(\xi)}_{\boldsymbol{k}_2,\nu_3} \hat{c}^{(\xi)}_{\boldsymbol{k}_1,\nu_4}, \quad (2)$$

where $V^{\{\nu_i\}\xi}_{\boldsymbol{k}_1,\boldsymbol{k}_2,\boldsymbol{q},\boldsymbol{G}} = V_{\boldsymbol{q}+\boldsymbol{G}} \mathcal{W}^{\xi\nu_1\nu_4}_{\boldsymbol{k}_1,\boldsymbol{q}+\boldsymbol{G}} \mathcal{W}^{\xi\nu_2\nu_3}_{\boldsymbol{k}_2,-\boldsymbol{q}-\boldsymbol{G}}$, with $i = 1,\ldots,4$, contains the screened Coulomb potential $V_{\boldsymbol{q}} = e^2/(2\epsilon_0 q A_M)[1 + \epsilon\coth(qd)]^{-1}$ for a gate separated from TBG by a dielectric of permittivity ϵ and thickness d, where ϵ_0 is the vacuum permittivity [Fig. 1(a)].

We focus on electron dynamics in its Floquet basis, treating interactions $\hat{H}_{\text{el-ph}}$ and $\hat{H}_{\text{el-el}}$ as weak perturbations scattering electrons between single-particle Floquet states [1–3,34,47]. The occupation probability $F^{(\xi)}_{\boldsymbol{k}\alpha}(t) = \langle \hat{f}^{(\xi)\dagger}_{\boldsymbol{k}\alpha}(t)\hat{f}^{(\xi)}_{\boldsymbol{k}\alpha}(t)\rangle$ is described by the Floquet-Boltzmann equation (FBE) [3,47–49],

$$\dot{F}^{(\xi)}_{\boldsymbol{k}\alpha}(t) = I^{\text{el-ph}}_{\boldsymbol{k}\alpha}[\{F^{(\xi)}_{\boldsymbol{k}\alpha}(t)\}] + I^{\text{el-el}}_{\boldsymbol{k}\alpha}[\{F^{(\xi)}_{\boldsymbol{k}\alpha}(t)\}]. \quad (3)$$

Here, $\hat{f}^{(\xi)\dagger}_{\boldsymbol{k}\alpha}(t)$ creates a single-particle electron state $|\Phi^{(\xi)}_{\boldsymbol{k}\alpha}(t)\rangle$, and $I^{\text{el-ph}}_{\boldsymbol{k}\alpha}$ and $I^{\text{el-el}}_{\boldsymbol{k}\alpha}$ are, respectively, the electron-phonon and electron-electron collision integrals, evaluated by the Fermi golden rule (see Supplemental Material for FBE details [50]). The steady-state distribution yields $\dot{F}^{(\xi)}_{\boldsymbol{k}\alpha} = 0$, and $\langle \hat{f}^{(\xi)\dagger}_{\boldsymbol{k}\alpha}(t)\hat{f}^{(\xi)}_{\boldsymbol{k}\alpha'}(t)\rangle$ is suppressed for $\alpha \neq \alpha'$ when $1/\tau^{\text{tot}}_{\boldsymbol{k}} \equiv 1/\tau^{\text{el}}_{\boldsymbol{k}} + 1/\tau^{\text{ph}}_{\boldsymbol{k}} \ll \Delta\varepsilon_{\boldsymbol{k}}/\hbar$, where $\tau^{\text{el}}_{\boldsymbol{k}}$ and $\tau^{\text{ph}}_{\boldsymbol{k}}$ are the interband electron-electron and electron-phonon scattering times, respectively, and $\Delta\varepsilon_{\boldsymbol{k}} = \min_{n\in\mathbb{Z}}|\varepsilon_{\boldsymbol{k}+} - \varepsilon_{\boldsymbol{k}-} + n\hbar\Omega|$ [47,49,53]. Because $\Delta\varepsilon_K = 2\Delta_K$ is minimal, the condition is equivalently $\zeta \equiv \hbar/(2\Delta_K\tau^{\text{tot}}_K) \ll 1$ [see Fig. 4(d)]. In Figs. 1(b), 4(c), and 4(d), we show the maximal ζ across fields $\mathcal{E}$ plotted in Figs. 1 and 3.

Transport properties.—To probe the electronic dynamics induced by the laser, we study the anomalous conductivity in the steady-state of the system [16,31–35,54–56]

$$\sigma_{xy} = \frac{2e^2}{\hbar} \sum_{\alpha,\xi=\pm} \int d^2\boldsymbol{k} \mathcal{B}^{(\xi)}_{\boldsymbol{k}\alpha} F^{(\xi)}_{\boldsymbol{k}\alpha}, \quad (4)$$

which averages the product of Berry curvature [16,41,57]

$$\mathcal{B}^{(\xi)}_{\boldsymbol{k}\alpha} = \frac{\Omega}{\pi}\int_0^{2\pi/\Omega} dt\, \mathrm{Im}\langle \partial_{k_x}\Phi^{(\xi)}_{\boldsymbol{k}\alpha}(t)|\partial_{k_y}\Phi^{(\xi)}_{\boldsymbol{k}\alpha}(t)\rangle, \quad (5)$$

and the steady-state fillings, $F^{(\xi)}_{\boldsymbol{k}\alpha}$. Without the drive, TBG has fragile topology with $\sigma_{xy}=0$ at charge neutrality [58–60]. The circularly polarized laser breaks time-reversal symmetry between the valleys $\xi=\pm1$, opens Haldane gaps in each valley, and produces nonzero σ_{xy}.

Our main finding is that σ_{xy} can be controlled by the field strength. It features a rapid drop as a function of the amplitude of the drive, $\mathcal{E}$, near the critical amplitude $\mathcal{E}^*$ [Fig. 1(b)]. This strong dependence on the external field indicates profound changes in the electronic steady-state distribution as the drive amplitude changes across $\mathcal{E}=\mathcal{E}^*$. Furthermore, this strong amplitude dependence arises only when the undriven effective electronic velocity v^0_{eff} is close to c_{ph} in TBG [Fig. 1(c)], a condition unique to TBG near the "slow-electron" regime [36,37].

Phenomenological analysis.—We explain the origin of the strong dependence of σ_{xy} on the drive amplitude near $\mathcal{E}=\mathcal{E}^*$ [Fig. 1(b)] by focusing on key processes affecting σ_{xy}, which involve momentum states (the K and K' points and resonance ring, see Fig. 2(c)] with large Berry curvature $\mathcal{B}^{(\xi)}_{\boldsymbol{k}\alpha}$. We assume that the steady-state occupation of the upper Floquet band (UFB, $\alpha=+$) and valley index ξ near K are uniform, $F^{(\xi)}_{\boldsymbol{k}+}=F^{(\xi)}_{K+}$, for $\boldsymbol{k}\in\mathcal{S}_K$, where $\mathcal{S}_K$ is a small circle enclosing the full-width half maximum of the Berry curvature peak at K [Fig. 2(c)].

The steady-state occupation emerges as a balance between the total incoming rate $\dot{F}^{(\xi)}_{K+}|_{\mathrm{in}}$ into $\mathcal{S}_K$ and outgoing rate $\dot{F}^{(\xi)}_{K+}|_{\mathrm{out}}$ from $\mathcal{S}_K$. Single phonon emission connecting the UFB $\mathcal{S}_{\mathrm{in}}$ [see Fig. 3(a)] with $\mathcal{S}_K$ is the dominant contribution to $\dot{F}^{(\xi)}_{K+}|_{\mathrm{in}}$. The two regions are connected by the phonon light cone [see Fig. 3(a)]. This rate is $\dot{F}^{(\xi)}_{K+}|_{\mathrm{ph,in}}\approx\mathcal{R}_{\mathrm{in}}(1-F^{(\xi)}_{K+})F^{(\xi)}_{\mathrm{in}}$, where $F^{(\xi)}_{\mathrm{in}}$ is the average UFB occupation in $\mathcal{S}_{\mathrm{in}}$, and $\mathcal{R}_{\mathrm{in}}$ is the average intrinsic scattering rate. Importantly, $\mathcal{R}_{\mathrm{in}}$ is proportional to the momentum-space area of $\mathcal{S}_{\mathrm{in}}$, denoted $\mathcal{A}_{\mathrm{in}}$, estimated by counting the UFB states that may scatter to $\mathcal{S}_K$ by electron-phonon interactions. Hence, $\mathcal{S}_{\mathrm{in}}$ is the intersection between the UFB and phonon light cones originating anywhere within $\mathcal{S}_K$ [Fig. 3(a)]. As Δ_R and Δ_K widen with $\mathcal{E}$, the Floquet bands become narrower [19,24,25], and $\mathcal{A}_{\mathrm{in}}$ shrinks, vanishing at $\mathcal{E}=\mathcal{E}^*$ [Fig. 3(b)]. The critical strength $\mathcal{E}^*$ is defined by $v_{\mathrm{eff}}(\mathcal{E}^*)=c_{\mathrm{ph}}$, where $v_{\mathrm{eff}}(\mathcal{E})=\max_{\boldsymbol{k}'}(\varepsilon^{(\xi)}_{\boldsymbol{k}'+}-\varepsilon^{(\xi)}_{\boldsymbol{K}+})/|\boldsymbol{k}'-\boldsymbol{K}|$ is the electronic velocity near the K point. By estimating $v_{\mathrm{eff}}(\mathcal{E})$, one finds that $\mathcal{E}^*\propto[1-c_{\mathrm{ph}}/v^0_{\mathrm{eff}}]^{\gamma}$ for small $1-c_{\mathrm{ph}}/v^0_{\mathrm{eff}}$, where γ depends on the quasienergy structure and $v^0_{\mathrm{eff}}\equiv v_{\mathrm{eff}}(0)$. One can also show $\mathcal{A}_{\mathrm{in}}\propto\max(\mathcal{E}-\mathcal{E}^*,0)$ as $\mathcal{E}\to\mathcal{E}^*$. (See Supplemental Material [50]).

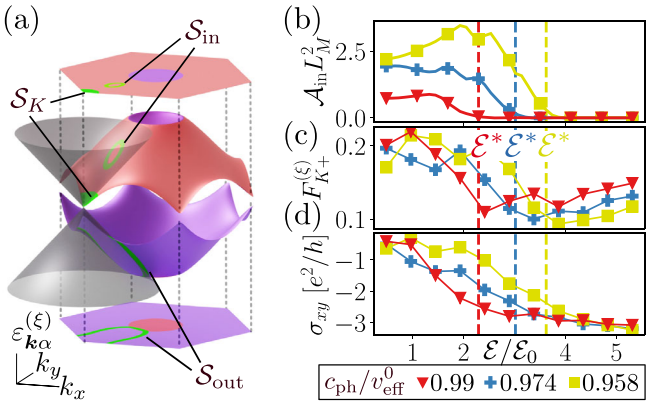

FIG. 3. (a) Schematics of the Floquet spectrum and one of the phonon light-cones originating from the area $\mathcal{S}_K$ in the UFB. The intersection between the UFB (LFB) and all cones centered in $\mathcal{S}_K$ form $\mathcal{S}_{\mathrm{in}}$ ($\mathcal{S}_{\mathrm{out}}$). As $\mathcal{E}\to\mathcal{E}^*$, the area of $\mathcal{S}_{\mathrm{in}}$ vanishes. (b)–(d) Numerical verification of the phenomenological model. (b) Area of $\mathcal{S}_{\mathrm{in}}$, $\mathcal{A}_{\mathrm{in}}$, vs $\mathcal{E}$ for three values of $c_{\mathrm{ph}}/v^0_{\mathrm{eff}}$. (c) Average occupation in $\mathcal{S}_K$. (d) Anomalous Hall conductivity σ_{xy} for same parameters as (b),(c). At $\mathcal{E}^*$ (dashed lines), $\mathcal{A}_{\mathrm{in}}$, $F^{(\xi)}_{K+}$, and σ_{xy} sharply change.

Similarly, the phonon-mediated outgoing rate is $\dot{F}^{(\xi)}_{K+}|_{\mathrm{ph,out}}\approx\mathcal{R}_{\mathrm{out}}F^{(\xi)}_{K+}(1-F^{(\xi)}_{\mathrm{out}})$, where $F^{(\xi)}_{\mathrm{out}}$ is the lower Floquet band (LFB, $\alpha=-$) average occupation in $\mathcal{S}_{\mathrm{out}}$, and $\mathcal{R}_{\mathrm{out}}$ is the average intrinsic rate, proportional to $\mathcal{A}_{\mathrm{out}}=\int_{\mathcal{S}_{\mathrm{out}}}d^2\boldsymbol{k}$, where $\mathcal{S}_{\mathrm{out}}$ is the momentum region enclosing intersections between the LFB with phonon light cones originating from states in $\mathcal{S}_K$ [see Fig. 3(a)]. However, unlike $\mathcal{A}_{\mathrm{in}}$, $\mathcal{A}_{\mathrm{out}}$ does not vanish as $\mathcal{E}\to\mathcal{E}^*$ and instead expands as $\mathcal{E}$ increases.

Electron-electron interactions and photon-mediated Floquet-umklapp (FU) processes introduce additional terms in the rate equation depending smoothly on $\mathcal{E}$ and roughly uniformly-spread in momentum. We thus include an incoming $\dot{F}^{(\xi)}_{K+}|_{r,\mathrm{in}}=\Gamma_{\mathrm{in}}(1-F^{(\xi)}_{K+})$ and outgoing rate $\dot{F}^{(\xi)}_{K+}|_{r,\mathrm{out}}=\Gamma_{\mathrm{out}}F^{(\xi)}_{K+}$ with $\Gamma_{\mathrm{in/out}}\equiv\Gamma^{\mathrm{ph}}_{\mathrm{in/out}}+\Gamma^{\mathrm{el}}_{\mathrm{in/out}}$, where $\Gamma^{\mathrm{el(ph)}}_{\mathrm{in/out}}$, are rates of electron-electron (electron-phonon FU) processes. The strength of FU processes is weaker than $\mathcal{R}_{\mathrm{out}}$ by factors of $\approx(v_F e\mathcal{E}/\Omega^2)^{2n}$, where $|n|>1$ is the number of photons emitted or absorbed [3]. FU processes also impart large phonon momentum transfers that the form-factor in Eq. (1) suppresses.

In the steady-state, $\dot{F}^{(\xi)}_{K+}|_{\mathrm{in}}=\dot{F}^{(\xi)}_{K+}|_{\mathrm{ph,in}}+\dot{F}^{(\xi)}_{K+}|_{r,\mathrm{in}}$ and $\dot{F}^{(\xi)}_{K+}|_{\mathrm{out}}=\dot{F}^{(\xi)}_{K+}|_{\mathrm{ph,out}}+\dot{F}^{(\xi)}_{K+}|_{r,\mathrm{out}}$ are equal, and

$$F^{(\xi)}_{K+}=\frac{\mathcal{R}_{\mathrm{in}}F^{(\xi)}_{\mathrm{in}}+\Gamma_{\mathrm{in}}}{\mathcal{R}_{\mathrm{in}}F^{(\xi)}_{\mathrm{in}}+\mathcal{R}_{\mathrm{out}}(1-F^{(\xi)}_{\mathrm{out}})+\Gamma_{\mathrm{in}}+\Gamma_{\mathrm{out}}}. \quad (6)$$

Note that $F^{(\xi)}_{\text{in}}$, $1 - F^{(\xi)}_{\text{out}} \neq 0$ due to electron (hole) excitations in the UFB (LFB) generated by FU processes. Since $\mathcal{R}_{\text{in}} \propto \mathcal{A}_{\text{in}}$, $\mathcal{R}_{\text{in}}$ decreases as a function of $\mathcal{E}$, shrinking to zero for $\mathcal{E} \geq \mathcal{E}^*$ [see Fig. 3(b) for numerical verification]. We expect a similar $\mathcal{E}$ dependence of $F^{(\xi)}_{K+}$ and σ_{xy}, yet smeared by additional scattering rates appearing in Eq. (6), as verified numerically in Fig. 1(b). Additionally, Eq. (6) elucidates the dependence of $F^{(\xi)}_{K+}$ on the ratio $\chi \equiv \tau^{\text{el}}_K/\tau^{\text{ph}}_K \approx \mathcal{R}_{\text{out}}/\Gamma^{\text{el}}_{\text{out}} \approx \mathcal{R}_{\text{out}}/\Gamma^{\text{el}}_{\text{in}}$ [see Fig. 1(b)], with $F^{(\xi)}_{K+} \to 0.5$ as $\chi \to 0$. In Figs. 1(b), 4(b), and 4(c), we display χ evaluated at the amplitude $\mathcal{E}$ where ζ is fixed.

A similar rate equation can be derived for the occupation probability of holes in the LFB. Because of the emergent, approximate antiunitary particle-hole symmetry [61–63] at charge neutrality that is preserved by the drive, the transition rates in the LFB are roughly similar to those in the UFB, leading to approximately equal electron and hole occupations near the Dirac points in the UFB and LFB ($F^{(\xi)}_{K+} \approx 1 - F^{(\xi)}_{K'-}$). Notice that the signs of the Berry curvatures near the Dirac points in the LFB and UFB are opposite, resulting in constructive contributions of electron and hole populations to σ_{xy}. Thus, we can reproduce qualitatively the sharp change of σ_{xy} with $\mathcal{E}$ in Fig. 3 [24]. Occupations in the resonance ring vicinity [Fig. 2(c)] yield a similar $\mathcal{E}$ dependence, but with a much lower critical field (not visible for $\mathcal{E}$ plotted in Figs. 1 and 3) due to different effective electronic velocities near the resonance ring.

Numerical analysis.—The results in Figs. 3(b)–3(d) utilized a simplified toy model describing TBG as a tight-binding hexagonal lattice, similar to graphene [64], but with parameters tuned to match v_F and the Brillouin zone size of TBG. This model misses some subtle details but captures the interplay between electron and phonon velocities and the large Berry curvature at the Dirac points and resonance ring. The model represents only the central $\nu = \pm 1$ bands of the undriven band structure, but since the low drive angular frequency Ω is only resonant to these narrow bands, we can ignore the $|\nu| > 1$ bands—valid when θ is near the magic angle where the $|\nu| > 1$ and $\nu = \pm 1$ bands are well separated. In the Supplemental Material [50], we present the numerical analysis of a continuum model without electron-electron interactions [29,38,65], which yields qualitatively similar results, demonstrating that the controllable σ_{xy} is insensitive to model details. In the toy model, $v^0_{\text{eff}} = 18.9$ km/s, and we vary $c_{\text{ph}} \in [17.9\ \text{km/s}, 19.4\ \text{km/s}]$ in Fig. 1(c). In the range $c_{\text{ph}} < v^0_{\text{eff}}$, the drive induces the regime $c_{\text{ph}} > v_{\text{eff}}(\mathcal{E})$ for $\mathcal{E} > \mathcal{E}^*$. To capture the decaying overlap of the wave functions for momentum umklapp transitions, in the toy model, we take $\mathcal{W}^{\xi\nu\nu'}_{\boldsymbol{k},\boldsymbol{q}} \to \langle \xi\nu'\boldsymbol{k} + \boldsymbol{q} | \xi\nu\boldsymbol{k}\rangle e^{-l_w^2 q^2/4}$, with $l_w \approx L_M/(1.5\sqrt{3})$ representing the radius of Wannier orbitals localized to TBG layer alignment sites [46,50].

First, we show how solving the FBE [Eq. (3)] for the steady-state distribution verifies the phenomenological model. Consider the noninteracting limit by solving Eq. (3) for $F^{(\xi)}_{\boldsymbol{k}\alpha}$ with $\chi \to \infty$ ($I^{\text{el-el}}_{\boldsymbol{k}\alpha} = 0$). The left-half column of Fig. 4(a) shows the noninteracting steady-state distributions for a phonon bath temperature of 1 K and $c_{\text{ph}} = 0.99 v^0_{\text{eff}}$ in the $\mathcal{E} > \mathcal{E}^*$ and $\mathcal{E} < \mathcal{E}^*$ cases. When $\mathcal{E} > \mathcal{E}^*$ (left bottom quadrant), the Dirac points have reduced occupations (see zoom-in boxes) relative to when $\mathcal{E} < \mathcal{E}^*$ (left top quadrant), because incoming scattering rates into $\mathcal{S}_{K,K'}$ are suppressed (verifying the phenomenological model). Figure 3(c) shows the occupation near the K point, $F^{(\xi)}_{K+}$, as a function of $\mathcal{E}$ for three values of $c_{\text{ph}}/v^0_{\text{eff}}$ and verifies $\mathcal{A}_{\text{in}}$, $F^{(\xi)}_{K+}$, and σ_{xy} sharply change at the same critical field $\mathcal{E} = \mathcal{E}^*$. Heating induced by FU processes causes $F^{(\xi)}_{K+}$ to slowly increase with $\mathcal{E} > \mathcal{E}^*$ [see Eq. (6)].

Next, we quantify the strength of Coulomb screening necessary to stabilize the steady state, which depends on the balance between electron-phonon cooling processes and electron-electron heating processes. We include $I^{\text{el-el}}_{\boldsymbol{k}\alpha} \neq 0$ by taking finite χ. On the right-half column of Fig. 4(a), we show the resulting steady-state occupations, which is slightly closer to the hot steady-state $F^{(\xi)}_{\boldsymbol{k}\pm} = 0.5$ and has more smeared occupations than the noninteracting case [left half of Fig. 4(a)]. To quantify the effect of interactions on σ_{xy}, note that, in Fig. 1(b), σ_{xy} drops less rapidly with $\mathcal{E} < \mathcal{E}^*$ as χ decreases. We capture this behavior with the visibility parameter $\mathcal{V} \equiv -\max_{\mathcal{E}<\mathcal{E}^*} |\partial_{\mathcal{E}} \sigma_{xy}|/[(e^2/h)/\mathcal{E}_0]$. Figure 4(b) demonstrates how $\mathcal{V}$ increases with χ. Lastly, we relate χ and ζ to physical parameters in TBG. Figure 4(c) shows the

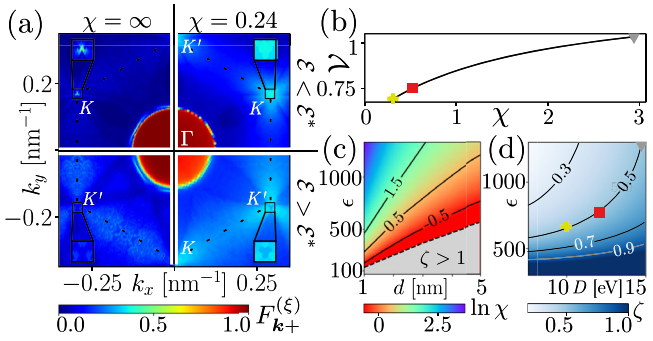

FIG. 4. (a) Left column: steady-state occupation of the UFB when $\chi = \infty$ (calculated on a 163×163 momentum grid). Right column: steady-state occupation when $\chi = 0.24$ (calculated on a 73×73 momentum grid). Bottom row: strong-drive case ($\mathcal{E} = 4.3\mathcal{E}_0 > \mathcal{E}^*$). Top row: weak-drive case ($\mathcal{E} = 0.97\mathcal{E}_0 < \mathcal{E}^*$). Enlarged boxes: the K, K' points have reduced occupation when $\mathcal{E} > \mathcal{E}^*$ relative to when $\mathcal{E} < \mathcal{E}^*$. (b) Visibility $\mathcal{V}$ vs χ. (c) Value of χ for various ϵ and gate distances d. (d) Value of η for various ϵ and deformation potentials D, with $d = 4$ nm. Points in (b),(d): parameters used in Fig. 1(b).

necessary gate distances d and dielectrics ϵ to experimentally achieve various values of χ, and Fig. 4(d) shows the values of ϵ and deformation potentials D satisfying $\zeta < 1$ for $d = 4$ nm. One suitable dielectric is $SrTiO_3$ with $\epsilon \sim 1600$ at $\Omega = 5$ meV$/\hbar$ angular frequencies [66–68]; note that surface optical phonons in $SrTiO_3$ are of higher frequencies than Ω and would not interact with electrons in TBG via direct (non-FU) scattering processes [69].

Conclusion.—TBG is a remarkable system whose Fermi velocity is comparable to the speed of sound. Upon THz-laser driving, the electronic population dynamics exhibits bottlenecks for electron-phonon scattering into high-Berry curvature Floquet states, strongly affecting the anomalous Hall transport. These bottlenecks can be sensitively controlled by the drive amplitude. If the undriven effective electron speed is faster than sound $v^0_{\mathrm{eff}} > c_{\mathrm{ph}}$, a drive with $\mathcal{E} > \mathcal{E}^*$ induces the opposite regime $v_{\mathrm{eff}}(\mathcal{E}) < c_{\mathrm{ph}}$, weakening the electron-phonon coupling and suppressing the Hall conductivity [Fig. 1(b)]. We also find that a strong $\mathcal{E}$ dependence of σ_{xy} arises for efficient Coulomb screening by a close-by gate or a strong dielectric [70–72]. Experimental advances in Floquet engineering [32], and THz laser sources [73,74], show that our predicitions should be accessible experimentally.

Analysis of UV-visible or x-ray driven TBG is a subject of future work, which must account for optically active dispersive bands [24,28]. High-frequency drives could reduce heating, facilitating fewer electron-electron FU processes [3] while activating electron-phonon umklapp cooling processes arising from tightly localized Wannier orbitals in TBG [46]. (In this Letter, these cooling processes are suppressed FU processes.) Another interesting direction involves developing a Hartree-Fock treatment for symmetry-broken phases in the steady-state of strongly coupled TBG [2]. We leave these exciting directions to future studies.

We thank Netanel Lindner, Mark Rudner, Or Katz, Gaurav Gupta, Seamus O'Hara, Jason Alicea, Alex Thomson, Felix von Oppen, Kryštof Kolář, Étienne Lantagne-Hurtubise, and Valerio Peri for valuable discussions. C. Y. gratefully acknowledges support from the DOE NNSA Stewardship Science Graduate Fellowship program, which is provided under cooperative Agreement No. DE-NA0003960. C. L. acknowledges support by the Gordon and Betty Moore Foundation's EPiQS Initiative, Grant GBMF8682, start-up funds from Florida State University and the National High Magnetic Field Laboratory. The National High Magnetic Field Laboratory is supported by the National Science Foundation through NSF/DMR-1644779 and the State of Florida. G. R. and I. E. are grateful for support from the Simons Foundation and the Institute of Quantum Information and Matter, as well as support from the NSF DMR Grant No. 1839271. This work is supported by ARO MURI Grant No. W911NF-16-1-0361, and was performed in part at the Aspen Center for Physics, which is supported by National Science Foundation Grant No. PHY-1607611.

[1] I. Esin, M. S. Rudner, and N. H. Lindner, Sci. Adv. **6**, 4922 (2020).
[2] I. Esin, G. Gupta, E. Berg, M. Rudner, and N. Lindner, Nat. Commun. **12**, 5299 (2021).
[3] K. I. Seetharam, C.-E. Bardyn, N. H. Lindner, M. S. Rudner, and G. Refael, Phys. Rev. B **99**, 014307 (2019).
[4] A. Castro, U. De Giovannini, S. A. Sato, H. Hübener, and A. Rubio, Phys. Rev. Res. **4**, 033213 (2022).
[5] D. Fausti, R. I. Tobey, N. Dean, S. Kaiser, A. Dienst, M. C. Hoffmann, S. Pyon, T. Takayama, H. Takagi, and A. Cavalleri, Science **331**, 189 (2011).
[6] N. Fläschner, B. S. Rem, M. Tarnowski, D. Vogel, D.-S. Lühmann, K. Sengstock, and C. Weitenberg, Science **352**, 1091 (2016).
[7] M. Nuske, L. Broers, B. Schulte, G. Jotzu, S. A. Sato, A. Cavalleri, A. Rubio, J. W. McIver, and L. Mathey, Phys. Rev. Res. **2**, 043408 (2020).
[8] S. Fazzini, P. Chudzinski, C. Dauer, I. Schneider, and S. Eggert, Phys. Rev. Lett. **126**, 243401 (2021).
[9] N. H. Lindner, G. Refael, and V. Galitski, Nat. Phys. **7**, 490 (2011).
[10] M. Vogl, S. Chaudhary, and G. A. Fiete, J. Phys. Condens. Matter **35**, 095801 (2022).
[11] I. A. Assi, J. P. F. LeBlanc, M. Rodriguez-Vega, H. Bahlouli, and M. Vogl, Phys. Rev. B **104**, 195429 (2021).
[12] M. Rodriguez-Vega, M. Vogl, and G. A. Fiete, Phys. Rev. Res. **2**, 033494 (2020).
[13] M. Vogl, M. Rodriguez-Vega, B. Flebus, A. H. MacDonald, and G. A. Fiete, Phys. Rev. B **103**, 014310 (2021).
[14] M. Liu, H. Y. Hwang, H. Tao, A. C. Strikwerda, K. Fan, G. R. Keiser, A. J. Sternbach, K. G. West, S. Kittiwatanakul, J. Lu, S. A. Wolf, F. G. Omenetto, X. Zhang, K. A. Nelson, and R. D. Averitt, Nature (London) **487**, 345 (2012).
[15] A. X. Gray *et al.*, Phys. Rev. B **98**, 045104 (2018).
[16] I. Esin, M. S. Rudner, G. Refael, and N. H. Lindner, Phys. Rev. B **97**, 245401 (2018).
[17] A. Kumar, M. Rodriguez-Vega, T. Pereg-Barnea, and B. Seradjeh, Phys. Rev. B **101**, 174314 (2020).
[18] H. Chono, K. Takasan, and Y. Yanase, Phys. Rev. B **102**, 174508 (2020).
[19] H. Dehghani, M. Hafezi, and P. Ghaemi, Phys. Rev. Res. **3**, 023039(R) (2021).
[20] J. Shan, M. Ye, H. Chu, S. Lee, J.-G. Park, L. Balents, and D. Hsieh, Nature (London) **600**, 235 (2021).
[21] E. L. Wong, A. J. Winchester, V. Pareek, J. Madéo, M. K. L. Man, and K. M. Dani, Sci. Adv. **4**, eaat9722 (2018).
[22] T. Kitagawa, T. Oka, A. Brataas, L. Fu, and E. Demler, Phys. Rev. B **84**, 235108 (2011).
[23] M. H. Michael, M. Först, D. Nicoletti, S. R. U. Haque, Y. Zhang, A. Cavalleri, R. D. Averitt, D. Podolsky, and E. Demler, Phys. Rev. B **105**, 174301 (2022).
[24] O. Katz, G. Refael, and N. H. Lindner, Phys. Rev. B **102**, 155123 (2020).

[25] Y. Li, H. A. Fertig, and B. Seradjeh, Phys. Rev. Res. **2**, 043275 (2020).
[26] G. E. Topp, G. Jotzu, J. W. McIver, L. Xian, A. Rubio, and M. A. Sentef, Phys. Rev. Res. **1**, 023031 (2019).
[27] M. Vogl, M. Rodriguez-Vega, and G. A. Fiete, Phys. Rev. B **101**, 241408(R) (2020).
[28] M. Vogl, M. Rodriguez-Vega, and G. A. Fiete, Phys. Rev. B **101**, 235411 (2020).
[29] R. Bistritzer and A. Macdonald, Proc. Natl. Acad. Sci. U.S.A. **108**, 12233 (2010).
[30] H. Dehghani, T. Oka, and A. Mitra, Phys. Rev. B **90**, 195429 (2014).
[31] H. Dehghani, T. Oka, and A. Mitra, Phys. Rev. B **91**, 155422 (2015).
[32] J. McIver, B. Schulte, F.-U. Stein, T. Matsuyama, G. Jotzu, G. Meier, and A. Cavalleri, Nat. Phys. **16**, 38 (2020).
[33] T. Oka and H. Aoki, Phys. Rev. B **79**, 081406(R) (2009).
[34] S. A. Sato, J. W. McIver, M. Nuske, P. Tang, G. Jotzu, B. Schulte, H. Hübener, U. De Giovannini, L. Mathey, M. A. Sentef, A. Cavalleri, and A. Rubio, Phys. Rev. B **99**, 214302 (2019).
[35] S. A. Sato, P. Tang, M. A. Sentef, U. D. Giovannini, H. Hübener, and A. Rubio, New J. Phys. **21**, 093005 (2019).
[36] I. Esin, I. Esterlis, E. Demler, and G. Refael, Phys. Rev. Lett. **130**, 147001 (2023).
[37] G. Sharma, I. Yudhistira, N. Chakraborty, D. Ho, M. Al Ezzi, M. Fuhrer, G. Vignale, and S. Adam, Nat. Commun. **12**, 5737 (2021).
[38] M. Koshino, N. F. Q. Yuan, T. Koretsune, M. Ochi, K. Kuroki, and L. Fu, Phys. Rev. X **8**, 031087 (2018).
[39] O. Karni, I. Esin, and K. M. Dani, Adv. Mater. **35**, 2204120 (2023).
[40] M. Rodriguez-Vega, M. Vogl, and G. Fiete, Ann. Phys. (Amsterdam) **435**, 168434 (2021).
[41] M. Rudner and N. Lindner, Nat. Rev. Phys. **2**, 229 (2020).
[42] M. Koshino and Y.-W. Son, Phys. Rev. B **100**, 075416 (2019).
[43] G. Usaj, P. M. Perez-Piskunow, L. E. F. Foa Torres, and C. A. Balseiro, Phys. Rev. B **90**, 115423 (2014).
[44] S. Aeschlimann, S. A. Sato, R. Krause, M. Chávez-Cervantes, U. De Giovannini, H. Hübener, S. Forti, C. Coletti, K. Hanff, K. Rossnagel, A. Rubio, and I. Gierz, Nano Lett. **21**, 5028 (2021).
[45] M. S. Rudner and N. H. Lindner, arXiv:2003.08252.
[46] H. Ishizuka, A. Fahimniya, F. Guinea, and L. Levitov, Nano Lett. **21**, 7465 (2021).
[47] K. I. Seetharam, C.-E. Bardyn, N. H. Lindner, M. S. Rudner, and G. Refael, Phys. Rev. X **5**, 041050 (2015).
[48] M. Genske and A. Rosch, Phys. Rev. A **92**, 062108 (2015).
[49] D. W. Hone, R. Ketzmerick, and W. Kohn, Phys. Rev. E **79**, 051129 (2009).
[50] See Supplemental Material at http://link.aps.org/supplemental/10.1103/PhysRevLett.131.026901 for details of derivations and numerical calculations, which includes Refs. [51,52].
[51] K. I. Seetharam, Thermalization in periodically-driven interacting quantum systems, Ph.D. thesis, California Institute of Technology, Pasadena, 2018.
[52] V. M. Galitskii and V. F. Elesin, J. Exp. Theor. Phys. **30**, 117 (1970).
[53] W. Kohn, J. Stat. Phys. **103**, 417 (2001).
[54] A. Chandran and S. L. Sondhi, Phys. Rev. B **93**, 174305 (2016).
[55] A. Tomadin, S. Diehl, and P. Zoller, Phys. Rev. A **83**, 013611 (2011).
[56] H. Dehghani and A. Mitra, Phys. Rev. B **93**, 245416 (2016).
[57] T. Fukui, Y. Hatsugai, and H. Suzuki, J. Phys. Soc. Jpn. **74**, 1674 (2005).
[58] K. Nuckolls, M. Oh, D. Wong, B. Lian, K. Watanabe, T. Taniguchi, B. Bernevig, and A. Yazdani, Nature (London) **588**, 610 (2020).
[59] C. Repellin and T. Senthil, Phys. Rev. Res. **2**, 023238 (2020).
[60] Y. Xie, A. Pierce, J. Park, D. Parker, E. Khalaf, P. Ledwith, Y. Cao, S. Lee, S. Chen, P. Forrester, K. Watanabe, T. Taniguchi, A. Vishwanath, P. Jarillo-Herrero, and A. Yacoby, Nature (London) **600**, 439 (2021).
[61] B. A. Bernevig, Z.-D. Song, N. Regnault, and B. Lian, Phys. Rev. B **103**, 205413 (2021).
[62] Z.-D. Song, B. Lian, N. Regnault, and B. A. Bernevig, Phys. Rev. B **103**, 205412 (2021).
[63] Z. Song, Z. Wang, W. Shi, G. Li, C. Fang, and B. A. Bernevig, Phys. Rev. Lett. **123**, 036401 (2019).
[64] Q. Chen, L. Du, and G. A. Fiete, Phys. Rev. B **97**, 035422 (2018).
[65] H. J. Monkhorst and J. D. Pack, Phys. Rev. B **13**, 5188 (1976).
[66] J. Ruhman and P. A. Lee, Phys. Rev. B **94**, 224515 (2016).
[67] H. Vogt and G. Rossbroich, Phys. Rev. B **24**, 3086 (1981).
[68] P. Dore, A. Paolone, and R. Trippetti, J. Appl. Phys. **80**, 5270 (1996).
[69] S. Saha, O. Kahya, M. Jaiswal, A. Srivastava, A. Annadi, J. Balakrishnan, A. Pachoud, C.-T. Toh, B.-H. Hong, J.-H. Ahn, T. Venkatesan, and B. Ozyilmaz, Sci. Rep. **4**, 6173 (2014).
[70] A. Coissard, D. Wander, H. Vignaud, A. G. Grushin, C. Repellin, K. Watanabe, T. Taniguchi, F. Gay, C. B. Winkelmann, H. Courtois, H. Sellier, and B. Sacépé, Nature (London) **605**, 51 (2022).
[71] L. Veyrat, D. Corentin, A. Coissard, X. Li, F. Gay, K. Watanabe, T. Taniguchi, Z. Han, B. Piot, H. Sellier, and B. Sacépé, Science **367**, 781 (2020).
[72] T. Sakudo and H. Unoki, Phys. Rev. Lett. **26**, 851 (1971).
[73] R. A. Lewis, J. Phys. D **47**, 374001 (2014).
[74] J. Costello, S. O'Hara, Q. Wu, D. Valovcin, L. Pfeiffer, K. West, and M. Sherwin, Nature (London) **599**, 57 (2021).